JOURNAL OF COMPUTATIONAL PHYSICS 98, 64–73 (1992)

Triangle Based Adaptive Stencils for the Solution of Hyperbolic Conservation Laws

LOUIS J. DURLOFSKY

Chevron Oil Field Research Company, P.O. Box 446, La Habra, California 90633-0446

AND

BJORN ENGQUIST* AND STANLEY OSHER*

Department of Mathematics, UCLA, Los Angeles, California 90024

Received January 3, 1990; revised December 7, 1990

A triangle based adaptive difference stencil for the numerical approximation of hyperbolic conservation laws in two space dimensions is constructed. The novelty of the resulting scheme lies in the nature of the preprocessing of the cell averaged data, which is accomplished via a nearest neighbor linear interpolation followed by a slope limiting procedure. Two such limiting procedures are suggested. The resulting method is considerably more simple than other triangle based non-oscillatory approximations which, like this scheme, approximate the flux up to second-order accuracy. Numerical results for constant and variable coefficient linear advection, as well as for nonlinear flux functions (Burgers' equation and the Buckley–Leverett equation), are presented. The observed order of convergence, after local averaging, is from 1.7 to 2.0 in L_1.

1. INTRODUCTION

In the last several years there has been considerable effort aimed at constructing and analyzing high order accurate, non-oscillatory approximations to hyperbolic conservation laws (see, e.g., [1–3]). It is by now well established that the spontaneous development of shock waves and the appearance of steep gradients in the solution require higher order schemes to have an adaptive stencil (by adaptive stencil we mean an adaptive flux approximation, *not* an adaptive grid) in order to suppress the spurious oscillations that plague conventional finite difference methods. Total variation diminishing (TVD) schemes, one such class of second-order accurate methods that eliminate unphysical oscillations, have been used successfully in a variety of applications. Recently, a new class of methods, essentially non-oscillatory (ENO) schemes [4, 5], which surpass the second-order accurate barrier associated with TVD schemes, has been developed. An alternative approach for third-order shemes was developed in [6].

Extensions of TVD and ENO schemes to two and three dimensions are typically designed in a dimension by dimension fashion. Therefore, the extension of these higher order schemes to the solution of hyperbolic conservation laws on unstructured grids, such as a triangular mesh, is not immediate. It is our intent in this paper to devise a second-order accurate scheme of TVD type (i.e., formally second-order accurate as a flux approximation and based on the MUSCL formulation [7, 8]) which is applicable to an unstructured triangular grid. Our scheme is based on a finite volume type discretization and is particularly straightforward to implement. The scheme relies on a very local adaptive interpolation idea, which results in computational efficiency. The adaptive two-dimensional interpolation ideas presented here can be extended to develop triangle based, higher order ENO type schemes. The application of the scheme to the simulation of two phase flow through porous media (e.g., oil reservoir simulation), considered briefly in Section 3, will be the subject of a future publication.

Several approaches for the solution of hyperbolic conservation laws on triangular grids already exist. A finite volume approach, with dissipation added explicitly, is discussed in [9]. Other techniques, within the context of finite element methods, have utilized flux corrected transport (FCT) ideas [10, 11] or have required the generation of a complex auxiliary grid [12] or are truly finite element methods in space and time and thus are more costly computationally [13, 14]. The methodology presented here is, in our opinion, simpler and more efficient, primarily because a finite volume rather than a finite element approach is used,

* Research supported by Chevron Oil Field Research Company, ONR Grant N00014-86-K-0691, NSF Grant DMS 88-11863, DARPA Grant in the ACMP program, NASA Langley Grant NAG1-270, and NASA University Consortium NCA-2372.

0021-9991/92 $3.00

thus avoiding the overhead associated with finite element schemes.

Although the methods we shall develop in Section 2 are multidimensional extensions of so-called second-order TVD schemes, they are technically neither total variation diminishing nor strictly second-order accurate (we will, however, refer to them as second-order schemes). In general, the total variation of our solutions may increase [15], though satisfaction of a maximum principle is achieved in all of our numerical calculations. Also, although the fluxes are strictly approximated up to second order, the truncation error is technically lower because of the adaptive stencil and the variable size of the triangles. Numerical experiments presented in Section 3 indicate orders of accuracy, after local averaging, between 1.7 and 2.0 in the L_1 norm. In Section 4 we suggest further extensions of the method within this context and indicate partial extensions to include diffusive terms.

2. CONSTRUCTION OF THE NUMERICAL SCHEMES

Our intent in this section is to develop a scheme to solve hyperbolic conservation laws on triangular grids in two space dimensions. The method presented is for a single hyperbolic conservation law, though hyperbolic systems can be treated analogously in a field by field manner (see, e.g., [4]). Our method is finite volume based and achieves greater than first-order accuracy through use of a novel adaptive flux interpolation procedure. We first present the general finite volume approach, then introduce our general limiting procedure, and then discuss various specific limiters.

2.1. *Finite Volume Discretization*

Consider the hyperbolic conservation law,

$$u_t + \nabla \cdot \mathbf{F}(u) = g(\mathbf{x}, t), \qquad u(\mathbf{x}, 0) = u_0(\mathbf{x}), \tag{2.1}$$

subject to boundary conditions. We wish to solve (2.1) on a triangular grid, a portion of which is shown schematically in Fig. 1. Integrating (2.1) over a triangle (Δ_{ABC} to be specific) gives

$$\frac{\partial}{\partial t}\int_{\Delta_{ABC}} u\, dA = -\int_{\Delta_{ABC}} (\nabla \cdot \mathbf{F})\, dA, \tag{2.2}$$

where Δ_{ABC} represents the region ABC, $|\Delta_{ABC}|$ denotes its area, and $g(\mathbf{x}, t)$ has been taken to be zero for simplicity of exposition only. Applying the divergence theorem to the right-hand side of (2.2) and defining

$$\bar{u}_{ABC} = \left(\int_{\Delta_{ABC}} u\, dA\right)(|\Delta_{ABC}|)^{-1},$$

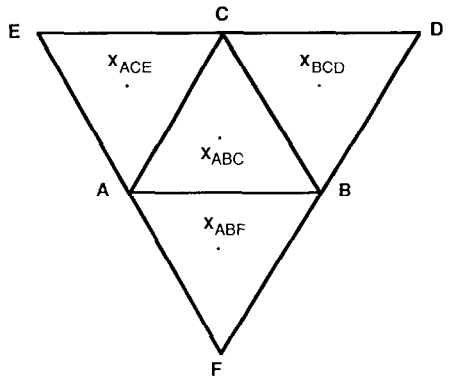

FIG. 1. Schematic of a portion of the triangular grid.

i.e., $\bar{u}_{ABC}$ the average of u over Δ_{ABC}, gives

$$\frac{\partial}{\partial t}\bar{u}_{ABC} = -\frac{1}{|\Delta_{ABC}|}\left[\int_{l_{AB}} \mathbf{F}\cdot\mathbf{n}_{AB}\, dl + \int_{l_{AC}} \mathbf{F}\cdot\mathbf{n}_{AC}\, dl + \int_{l_{BC}} \mathbf{F}\cdot\mathbf{n}_{BC}\, dl\right]. \tag{2.3}$$

Note that $\bar{u}_{ABC}$ is equal to the value of u evaluated at the triangle centroid ($\mathbf{x}_{ABC}$) to within $O(|\Delta_{ABC}|)$, or, analogously, to within $O(l^2)$, where l is the characteristic length of a side of Δ_{ABC}. Here $\mathbf{n}$ is the unit outward normal. We require that all angles be uniformly bounded away from zero.

We approximate (2.3) by first using a semi-discrete approach where the approximation is

$$v_{ABC}(t) \approx \bar{u}_{ABC}(t);$$

the same is true for all triangles. First-order accurate monotone schemes can easily be constructed—see, e.g., [16, 17]. Let $h_{BC}(w_1, w_2)$ be a two-point Lipschitz continuous monotone flux, approximating $\mathbf{F}\cdot\mathbf{n}_{BC}$, i.e.,

$$h_{BC}(w, w) = \mathbf{F}\cdot\mathbf{n}_{BC}, \tag{2.4a}$$

$$h_{BC}(w_1, w_2) \text{ is a nondecreasing function of } w_1 \text{ and a nonincreasing function of } w_2. \tag{2.4b}$$

Then our semidiscrete monotone approximation is

$$\frac{\partial}{\partial t}v_{ABC}(t) = -\frac{1}{|\Delta_{ABC}|}\left[h_{BC}(v_{ABC}, v_{BCD})\cdot l_{BC} + h_{AB}(v_{ABC}, v_{ABF})\cdot l_{AB} + h_{AC}(v_{ABC}, v_{ACE})\cdot l_{AC}\right], \tag{2.5}$$

where l_{BC} is the length of the side BC, etc. "E" schemes may also be used—see [16] for the definition and for examples.

In [18, Theorem 2-2], it was shown for monotone schemes of this type that a triangle based Lax–Wendroff type theorem is true. Precisely, we define the quantity

$$B(v) = \sum |v_{ABC}(t) - v_{A'B'C'}(t)|\, d,$$

where (1) the sum is taken over all values such that Δ_{ABC} and $\Delta_{A'B'C'}$ have a common edge, (2) the triangulation is such that the largest inscribed circle and the smallest circumscribed circle both have diameter which is uniformly $O(d)$, and (3) $B(v)$ is uniformly bounded for all t as the triangulation is refined, i.e., as $d \to 0$. Then, monotone schemes of the type (2.5) converge to a weak solution of (2.1). It is a straightforward matter to extend this result to the schemes we shall develop below.

To obtain higher order accuracy we preprocess our initial data so that in each triangle, in particular Δ_{ABC}, a linear function is obtained whose cell average equals v_{ABC}, but which is within $O(|\Delta|)$ of u_{ABC} in regions of smoothness. Here $|\Delta|$ is the maximum area of the four triangles seen in Fig. 1. Moreover, this linear function will not introduce new oscillations in our approximation. This (simple) construction is the key part of this paper; it will be described at the end of this section. We call this linear approximation $L_\Delta(\mathbf{x})$. It is generally discontinuous across the boundary of each triangle.

Let $\mathbf{x}_{BC}$ be the midpoint of side BC, etc. Let $L_\Delta(\mathbf{x}^i_{BC})$ denote the limit of $L_\Delta(\mathbf{x})$ as $\mathbf{x} \to \mathbf{x}_{BC}$ from *inside* triangle ABC and $L_\Delta(\mathbf{x}^0_{BC})$ denote the limit as $\mathbf{x} \to \mathbf{x}_{BC}$ from *outside* triangle ABC. Generally,

$$|L_\Delta(\mathbf{x}^i_{BC}) - L_\Delta(\mathbf{x}^0_{BC})| = O(|\Delta|).$$

Our second-order accurate, semi-discrete approximation to (2.3) is

$$\begin{aligned}\frac{\partial}{\partial t} v_{ABC}(t) = -\frac{1}{\Delta_{ABC}} [&h_{BC}(L_\Delta(\mathbf{x}^i_{BC}), L_\Delta(\mathbf{x}^0_{BC})) \cdot l_{BC} \\ &+ h_{AB}(L_\Delta(\mathbf{x}^i_{AB}), L_\Delta(\mathbf{x}^0_{AB})) \cdot l_{AB} \\ &+ h_{AC}(L_\Delta(\mathbf{x}^i_{AC}), L_\Delta(\mathbf{x}^0_{AC})) \cdot l_{AC}]. \end{aligned} \tag{2.6}$$

By the midpoint formula for integrals, this approximation is *weakly* second-order accurate, in the sense that each of the three flux terms above is within $O(|\Delta|)$ of the line integrals, $\int \mathbf{F} \cdot \mathbf{n}\, dl$, along the corresponding interfaces. However, due to the shifting stencil and varying size and relation of the triangles, the pointwise truncation error is generally only $O(|\Delta|^{1/2})$, i.e., first order. The performance appears to be around 1.7–2.0 order in L_1 (see Section 3).

2.2. *Construction of Linear Function L_Δ*

We now describe the construction of L_Δ. In each interior triangle, three candidates for L_Δ, designated L^i_Δ, are generated. The first such candidate L^1_Δ, is the linear interpolate of the three values

$$(\mathbf{x}_{ABC}, v_{ABC}), (\mathbf{x}_{BCD}, v_{BCD}), (\mathbf{x}_{ACE}, v_{ACE}),$$

L^2_Δ is the interpolation of

$$(\mathbf{x}_{ABC}, v_{ABC}), (\mathbf{x}_{BCD}, v_{BCD}), (\mathbf{x}_{ABF}, v_{ABF}),$$

and L^3_Δ the interpolation of

$$(\mathbf{x}_{ABC}, v_{ABC}), (\mathbf{x}_{ACE}, v_{ACE}), (\mathbf{x}_{ABF}, v_{ABF}).$$

These three linear interpolants are sketched in Fig. 2. Here and below we assume that the three triangle centroids are not colinear. At this point, three possible L^i_Δ exist, and a limited version of L_Δ must be selected from these. To accomplish this, we first compute the magnitude of the gradient of each L^i_Δ; i.e.,

$$\begin{aligned}&\left[\left(\frac{\partial}{\partial x_1} L^i_\Delta\right)^2 + \left(\frac{\partial}{\partial x_2} L^i_\Delta\right)^2\right]^{1/2} \\ &\quad \equiv |\nabla L^i_\Delta|, \qquad \text{for} \quad i = 1, 2, 3. \end{aligned} \tag{2.7}$$

By analogy with limiting procedures in one space dimension [19], a valid, non-compressive limiter corresponds to the selection of the L^i_Δ for which $|\nabla L^i_\Delta|$ is the minimum. This choice is analogous to the *min* limiter in second-order ENO methods [4]. At extrema (i.e., when v_{ABC} is an extremum relative to v_{ACE}, v_{BCD}, and v_{ABF}), a first-order approximation ($L_\Delta = v_{ABC}$) is used. This limiter is applicable to problems involving nonlinear flux functions.

It is desirable to construct a more compressive limiter than that described above for problems involving linear or contact discontinuities. To accomplish this, we first consider the more compressive slope limiters in one dimension, the Φ type limiters described by Sweby [19, Eq. (3.17)] of which superbee is the most compressive, corresponding to $\Phi = 2$. These limiters allow the use of piecewise linear approximations to the solution for which the slope is not the minimum,

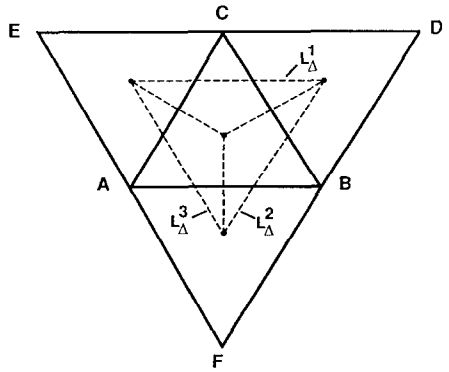

FIG. 2. Three candidates for the linear interpolation of v over Δ_{ABC}.

subject to the restriction that no overshoot (or undershoot) occurs at the cell boundaries.

The next limiter we describe is a multidimension analog of the one-dimensional Φ limiters. The approach here is to select the L_Δ^i for which $|\nabla L_\Delta^i|$ is maximized, subject to the restriction that no overshoot or undershoot occurs at any of the three triangle boundaries. The procedure is as follows:

(i) Select the L_Δ^i for which $|\nabla L_\Delta^i|$ is the maximum.

(ii) Check for overshoot or undershoot at $\mathbf{x}_{AB}$, $\mathbf{x}_{AC}$, and $\mathbf{x}_{BC}$. For L_Δ^i to represent a valid L_Δ, it suffices to verify that, for Δ_{ABC},

$$L_\Delta(\mathbf{x}_{AC}) \text{ is between } v_{ABC} \text{ and } v_{ACE},$$

$$L_\Delta(\mathbf{x}_{AB}) \text{ is between } v_{ABC} \text{ and } v_{ABF},$$

$$L_\Delta(\mathbf{x}_{BC}) \text{ is between } v_{ABC} \text{ and } v_{BCD}.$$

If these three requirements are satisfied, L_Δ^i is the appropriate L_Δ.

(iii) If the L_Δ^i above results in overshoot or undershoot at any one of the three midpoints, select the L_Δ^i for which $|\nabla L_\Delta^i|$ is the second largest and repeat the test in (ii). If this L_Δ^i does not satisfy the test in (ii), select the L_Δ^i for which $|\nabla L_\Delta^i|$ is the minimum.

Extrema are treated as described above.

Given L_Δ, the right-hand side of (2.6) can be evaluated and $v_{ABC}(t)$ integrated in time. This time integration is accomplished via a second-order TVD Runge–Kutta procedure [20].

3. NUMERICAL VERIFICATION OF HIGHER ORDER SCHEME

In this section we present results for the convergence of the general method described in Section 2, as well as solution contours and profiles demonstrating the accuracy of the method. In all cases, the solution region is a square domain discretized via right triangular "volumes" (referred to as elements), as shown in Fig. 3. Periodic boundary conditions are imposed in both the x- and the y-directions; the initial condition is similarly x- and y-periodic unless otherwise noted.

3.1. *Rate of Convergence*

The rate of convergence of the scheme is now assessed for both linear and nonlinear flux functions. We first consider solution of the linear conservation law

$$u_t + \nabla \cdot (\mathbf{a}u) = 0, \tag{3.1}$$

subject to the initial condition

$$u_0(x, y) = \sin(2\pi x)\sin(2\pi y). \tag{3.2}$$

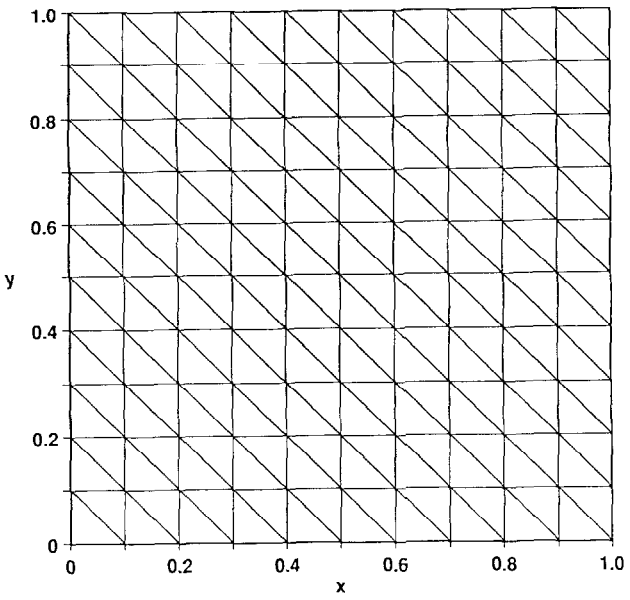

FIG. 3. Triangular grid used for the numerical calculations.

Our base monotone scheme uses the EO flux [16]:

$$h(w_1, w_2) = f_+(w_1) + f_-(w_2). \tag{3.3}$$

For linear equations with constant $\mathbf{a} = (a_1, a_2)$,

$$f_+(u) = [\max((\mathbf{a}\cdot\mathbf{n}), 0)]u, \tag{3.4a}$$

$$f_-(u) = [\min((\mathbf{a}\cdot\mathbf{n}), 0)]u. \tag{3.4b}$$

For Burgers' equation (considered below), where $f_1 = f_2 = (\frac{1}{2})u^2$ (f_1 and f_2 are the components of $\mathbf{F}$),

$$f_+(u) = u \max\left(\left(\frac{n_1+n_2}{2}\right)u, 0\right), \tag{3.5a}$$

$$f_-(u) = u \min\left(\left(\frac{n_1+n_2}{2}\right)u, 0\right), \tag{3.5b}$$

where n_1 and n_2 represent the components of $\mathbf{n}$.

A contour plot of the initial condition (3.2) is shown in Fig. 4. Four extrema are evident. The rate of convergence of the method was determined for both the case $a_x = a_y = 1$ and $a_x = 1$, $a_y = 0$. The solution of (3.1) was achieved using the more compressive limiter described above. Convergence was assessed both on an element by element basis and after applying a local averaging procedure. It is expected that local averaging procedures would enhance the rate of convergence, as the scheme is expected to be second order in only the weak sense, i.e., after integrating locally in space and time (a type of local averaging). The averaging performed in this study is, however, only spatial; no temporal averaging is attempted. This is because spatial–temporal

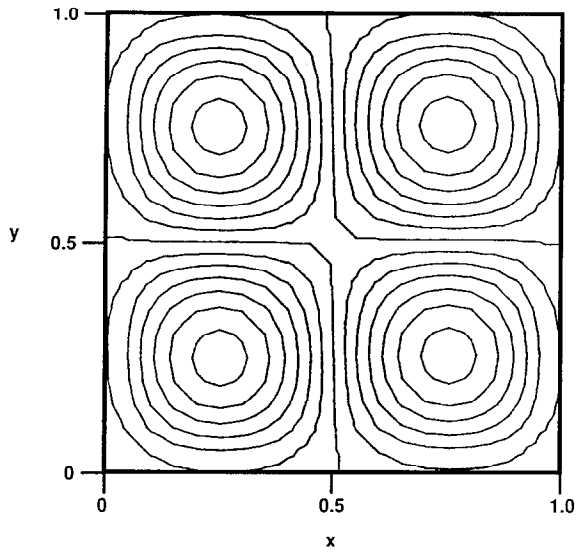

FIG. 4. Contour plot of the initial condition (3.2). Contours correspond to $u = 0, \pm 0.15, \pm 0.3, \pm 0.45, \pm 0.6, \pm 0.75, \pm 0.9$.

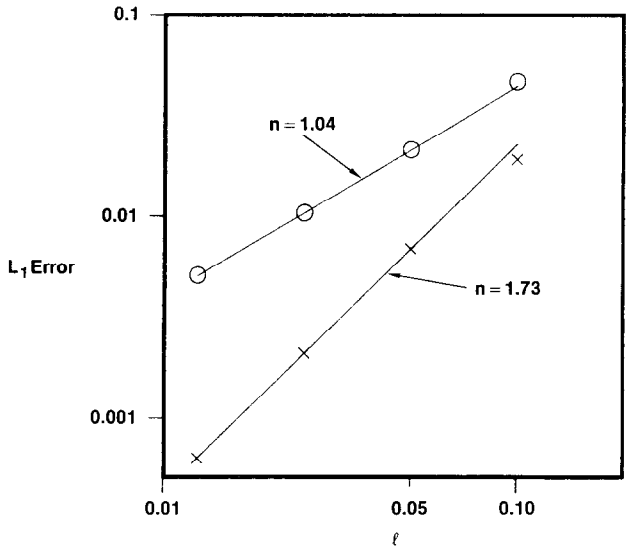

FIG. 6. L_1 error after local averaging for the case $a_x = 1$, $a_y = 0$ for first-order (○) and second-order (×) schemes. Lines are least square fits with slopes as indicated.

averages are rather cumbersome to perform in practice, and the spatial averaging alone reveals the expected trend. Computations were performed for grids ranging in discretization from 200 elements ($l = 0.1$, where l is the spacing between adjacent nodes or, analogously, $l = (2\Delta)^{1/2}$, with Δ the area of any element) to 12,800 elements ($l = 0.0125$). In all cases the CFL number, $\lambda (= \Delta t/l)$, was set to 0.1.

Displayed in Fig. 5 is a log–log plot of L_1 error versus l. In this case, $a_x = 1$, $a_y = 0$. Results are shown for both a first-order scheme and the higher order scheme, with error computed on an element by element basis. Least squares linear fits (for $l < 0.1$) give the order of convergence, designated n, for the two methods; for the first-order method we obtain 0.99 and for the higher order method 1.55. Figure 6 displays an analogous plot after applying a local averaging procedure. Specifically, this averaging procedure entails averaging the computed value of u over square regions comprised of two adjacent elements and computing the error in terms of the difference between this average and the exact solution of Eq. (3.1) evaluated at the square midpoint. For the grid displayed in Fig. 3, 100 such square regions

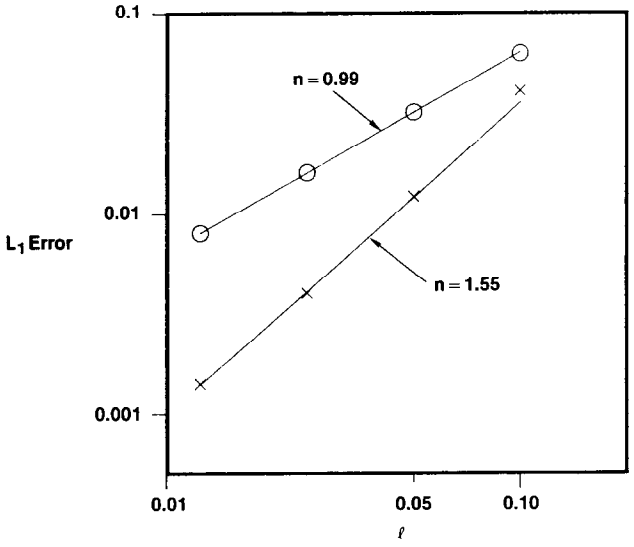

FIG. 5. L_1 error on a per element basis for the case $a_x = 1$, $a_y = 0$ for first-order (○) and second-order (×) schemes. Lines are least square fits with slopes as indicated.

TABLE I

Computed Accuracies for the Linear Case

Scheme	Norm	# elements	n
$a_x = a_y = 1$			
2nd O	L_1	1	1.75
2nd O	L_1	2	1.78
2nd O	L_2	1	1.61
2nd O	L_2	2	1.59
2nd O	L_∞	1	1.08
2nd O	L_∞	2	1.20
1st O	L_1	1	0.95
1st O	L_1	2	0.95
1st O	L_2	1	0.96
1st O	L_2	2	0.96
1st O	L_∞	1	0.98
1st O	L_∞	2	0.96
$a_x = 1$, $a_y = 0$			
2nd O	L_1	1	1.55
2nd O	L_1	2	1.73
1st O	L_1	1	0.99
1st O	L_1	2	1.04

Note. Initial condition $u_0(x, y) = \sin(2\pi x)\sin(2\pi y)$. Error computed over the entire domain.

TABLE II

Computed Accuracies (L_1) for the Linear Case

Scheme	#elements	n
$a_x = a_y = 1$		
2nd O	1	1.85
2nd O	2	1.87
$a_x = 0, a_y = 1$		
2nd O	1	1.22
2nd O	2	1.80
1st O	1	0.99
1st O	2	1.10

Note. Initial condition $u_0(x, y) = \sin(\pi x/2)\sin(\pi y/2)$ contains no extrema. Error computed over $0.6 \leqslant x, y \leqslant 0.8$ at $t = 0.05$.

exist. Again, averaging is only applied spatially; no temporal averaging is performed. Assessing error in this manner results in least squares linear fits of slope 1.04 for the first-order method and 1.73 for the higher order method. As expected, local averaging enhances the rate of convergence though, in this case, the improvement is not that substantial. In other cases, however, the improvement is more significant (see below).

Shown in Table I is a compilation of the rates of convergence for both the cases $a_x = a_y = 1$ and $a_x = 1$, $a_y = 0$. Results for both a first-order scheme and our more accurate scheme are displayed. In all cases the initial condition is as in (3.2). Error is computed over the entire domain in two ways: (1) element by element (#elements = 1); (2) by combining two adjacent elements into squares (#elements = 2). For the case $a_x = a_y = 1$, results for L_2 and L_∞ error are also shown. After local averaging, L_1 error $\sim O(l^{1.78})$, L_2 error $\sim O(l^{1.59})$, and L_∞ error $\sim O(l^{1.20})$. These results are analogous to those of second-order TVD schemes in one dimension, for which L_1 error $\sim O(l^2)$, L_2 error $\sim O(l^{1.5})$, and L_∞ error $\sim O(l)$, where l is a typical grid spacing.

Slightly improved rates of convergence in L_1 are obtained when the initial condition contains no extrema. This is demonstrated in Table II, where results for L_1 error for the initial condition $u_0(x, y) = \sin(\pi x/2)\sin(\pi y/2)$ are displayed. Here, to eliminate the effects of the discontinuity in u at the boundary (recall that periodic boundary conditions are imposed), error is computed only over the region $0.6 \leqslant x, y \leqslant 0.8$ at an early time, $t = 0.05$. In one case, local averaging has a more dramatic effect, improving the L_1 accuracy of the scheme from 1.22 to 1.80.

We next assess the rate of convergence of the scheme for a nonlinear flux function, $f_1 = f_2 = \frac{1}{2}u^2$ in Eq. (2.1) (i.e., the inviscid Burgers' equation). The initial condition is here taken as $u_0(x, y) = \sin(2\pi x)$; this problem is therefore essentially one-dimensional. For this case we apply the less compressive *min* limiter described in Section 2.2 (this limiter is more appropriate for nonlinear flux functions). Away from extrema, convergence in L_1 is $O(1.98)$ with local averaging and $O(1.95)$ on an element by element basis. For the first-order scheme, the analogous rates of convergence are $O(1.00)$ and $O(0.98)$, respectively. Over the entire domain, the convergence of our scheme in L_1 is $O(1.89)$ with local averaging and $O(1.82)$ on an element by element basis. The analogous first-order results are $O(1.00)$ and $O(0.95)$. Solution profiles for this essentially one-dimensional problem, computed using our scheme with 80 elements in the x-direction, are shown in Fig. 7. No overshoot or unphysical oscillations appear in the solution.

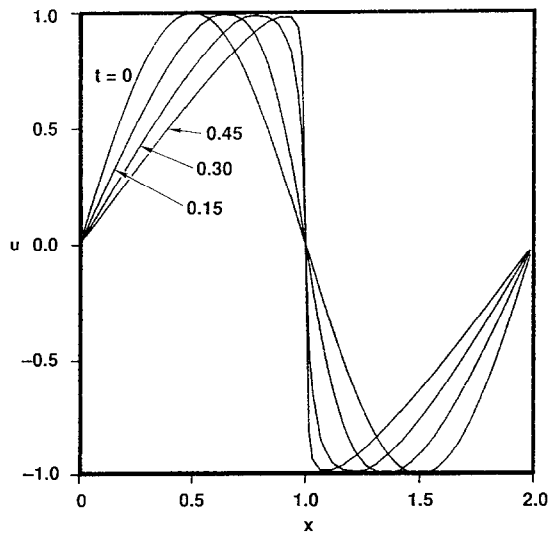

FIG. 7. Solution profiles for Burgers' equation using second-order scheme (80 elements in x-direction).

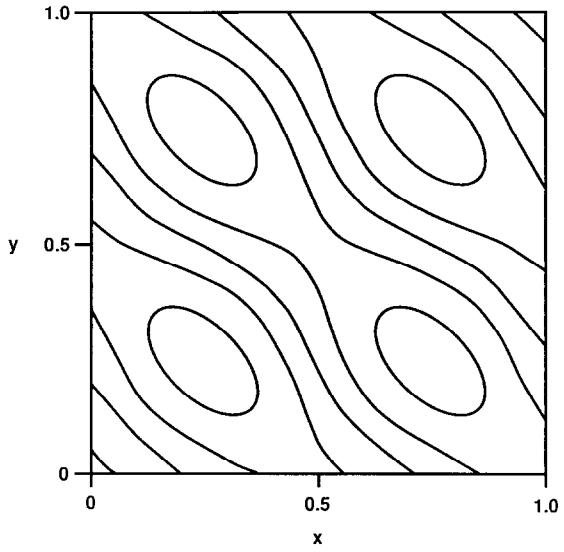

FIG. 8. Results for first-order scheme with 800 elements at $t = 1$. Contours correspond to $u = 0, \pm 0.1, \pm 0.2$.

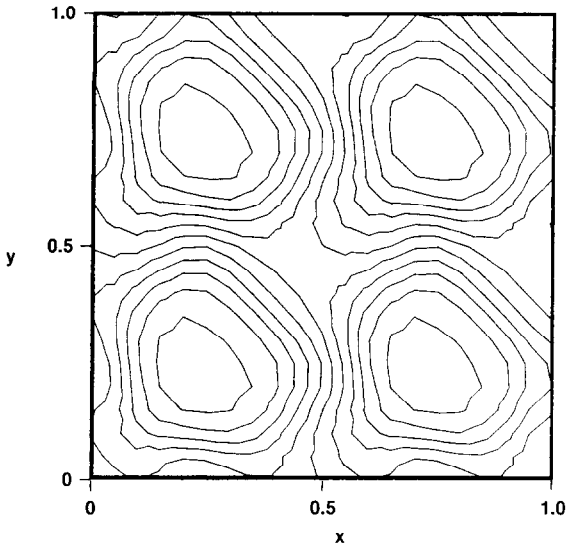

FIG. 9. Results for second-order scheme with 800 elements at $t = 1$. Contours correspond to $u = 0, \pm 0.15, \pm 0.3, \pm 0.45, \pm 0.6, \pm 0.75$.

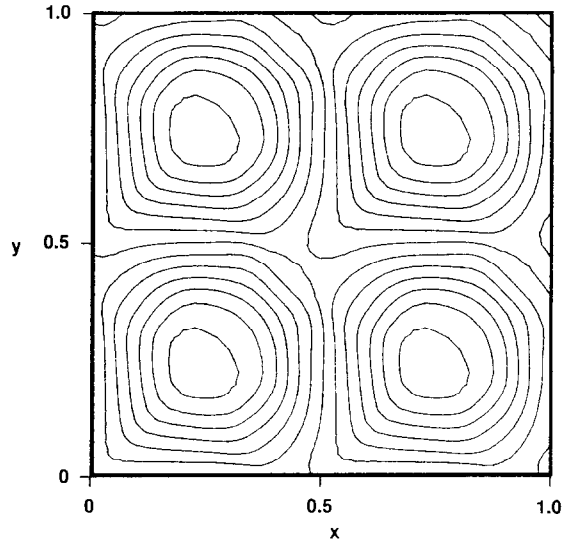

FIG. 11. Results for second-order scheme with 3200 elements at $t = 1$. Contours correspond to $u = 0, \pm 0.15, \pm 0.3, \pm 0.45, \pm 0.6, \pm 0.75, \pm 0.9$.

Based on the numerical results presented above and the analysis presented in Section 2, the method has been shown to be of greater than first-order accuracy. Observed convergence, after local averaging, ranged from $O(1.7)$ to $O(2.0)$ in L_1.

3.2. *Examples of Numerical Accuracy*

We now present some detailed numerical results for our higher order scheme and compare these with the results of a first-order method. The first results are for the solution of Eqs. (3.1) and (3.2) with $a_x = a_y = 1$. Figure 8 displays the solution contour results for the first-order scheme with 800 elements ($l = 0.05$) and $\lambda = 0.1$ (the same CFL number is used in all computations) at $t = 1$. The exact solution is a reproduction of the initial condition, shown in Fig. 4. The first-order method is clearly very diffusive; the maximum value of u is here only 0.25, in contrast to the maximum in the initial condition of 1. Results for the second-order scheme, using the more compressive limiter, at $t = 1$ are shown in Fig. 9. Though some distortion of the initial condition is apparent, the solution is considerably improved over the first-order solution; the maximum value of u is now 0.81. Shown in Fig. 10 are the $t = 1$ results for the first-order scheme using 3200 elements ($l = 0.025$). Substantial numerical diffusion is still evident; the maximum value of u is only 0.49. The solution contour using the second-order method is displayed in Fig. 11. The $t = 1$ solution in this case closely resembles the initial condition, with a maximum value of u of 0.94. Figures 12 and 13 show solution profiles taken along the line $y = x$ (the velocity direction) at $t = 0, 0.25, 0.5, 0.75,$

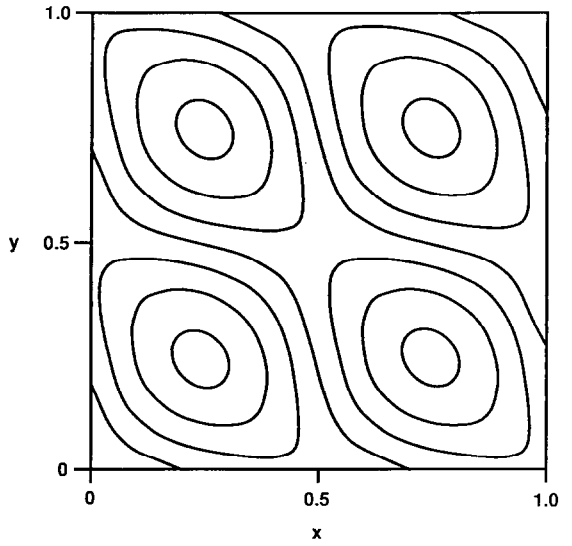

FIG. 10. Results for first-order scheme with 3200 elements at $t = 1$. Contours correspond to $u = 0, \pm 0.15, \pm 0.3, \pm 0.45$.

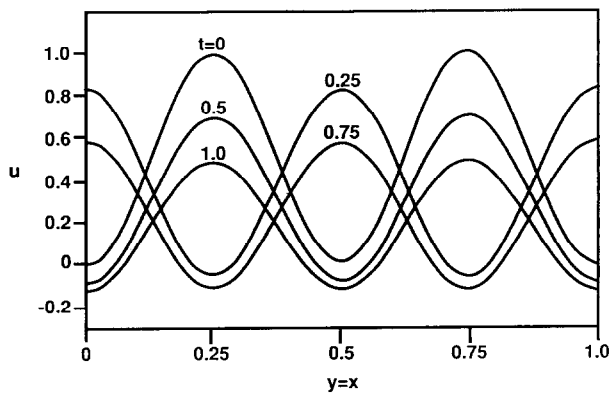

FIG. 12. Solution profiles along the line $y = x$ for the first-order scheme (3200 elements).

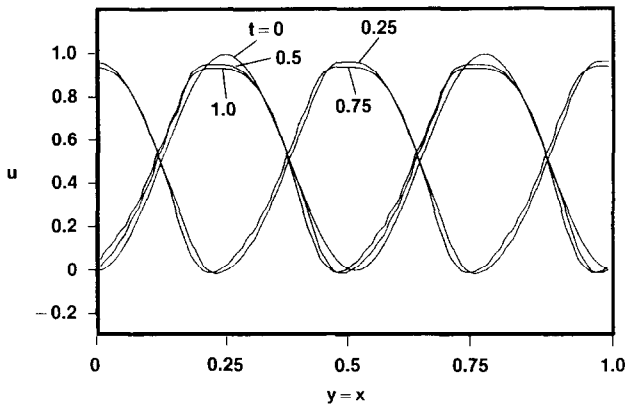

FIG. 13. Solution profiles along the line $y = x$ for the second-order scheme (3200 elements).

and 1 for both the first- and second-order methods. In both cases, 3200 elements were used. The second-order results are quite sharp at all times, while the first-order results show a continual degradation with increasing time.

We next consider solution of the rotating cone problem, a variable coefficient linear advection problem. The initial condition, shown in Fig. 14, is a cone of maximum height 1 and radius 0.15, centered at $x = 0.75$, $y = 0.5$. We set $a_x = -(y - 0.5)$, $a_y = (x - 0.5)$ in Eq. (3.1). The exact solution is counterclockwise rotation of the initial condition about $x = 0.5$, $y = 0.5$. The solution after half of a revolution attained via the first-order method with 3200 elements is shown in Fig. 15. The maximum in u is here only 0.48, reduced from 1 in the initial condition. The solution using the higher order method, again with 3200 elements, is shown in Fig. 16. The limiter used here is again the more

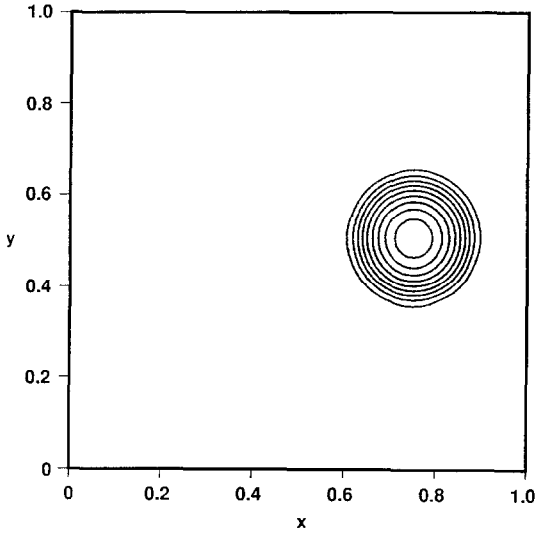

FIG. 14. Contour plot of the initial condition for rotating cone problem. Contours correspond to $u = 0$, 0.1, 0.2, 0.3, 0.4, 0.5, 0.6, 0.7, 0.8, 0.9.

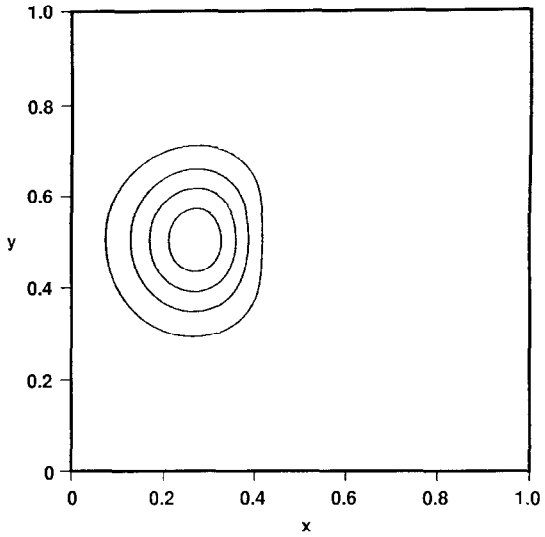

FIG. 15. Results for first-order scheme with 3200 elements after $\frac{1}{2}$ revolution. Contours correspond to $u = 0$, 0.1, 0.2, 0.3, 0.4.

compressive limiter described in Section 2.2. The solution is greatly improved over that achieved by the first-order method; the maximum in u is here 0.88.

The last example considered is the Buckley–Leverett equation describing two phase flow through porous media (e.g., water displacing oil),

$$u_t + \nabla \cdot [\mathbf{a} f(u)] = 0, \tag{3.6}$$

where u refers to the saturation of one of the fluids (water), $\mathbf{a}$ represents the two-dimensional velocity field and $f(u)$ is a typically nonconvex function derived from laboratory measurements. Here we take

$$f = \frac{u^2}{0.2 - 0.4u + 1.2u^2}. \tag{3.7}$$

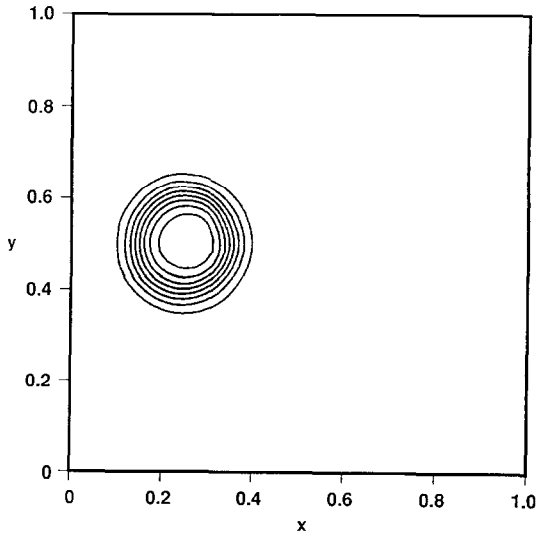

FIG. 16. Results for second-order scheme with 3200 elements after $\frac{1}{2}$ revolution. Contours correspond to $u = 0$, 0.1, 0.2, 0.3, 0.4, 0.5, 0.6, 0.7, 0.8.

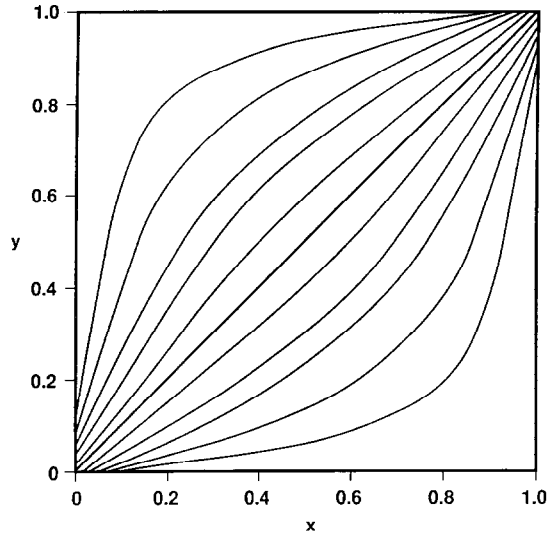

FIG. 17. Initial streamlines for flow in a quarter five spot geometry.

Solution of (3.6) is complicated by the fact that the velocity field, determined by Darcy's law, is dependent on the water saturation u and therefore evolves in time. See [21] for details.

We solve (3.6) using the *min* limiter described in Section 2.2 on a 200-element grid with initial condition $u_0 = 0$. Water is continuously injected in the lower left-hand corner ($u = 1$) and fluids produced in the upper right-hand corner; no flow boundary conditions are imposed elsewhere. This specification corresponds to one quarter of a five spot production pattern. The velocity field is computed at each time step through an accurate finite element solution of the so-called pressure equation. Streamlines for the initial velocity field are shown in Fig. 17; this velocity field is continuously modified as the displacement progresses. Solution contours at a later time are shown in Fig. 18. Note the relatively sharp front near the production region and the rarefaction behind the front. Both these regions of the solution are better defined with our higher order method than with the first-order method.

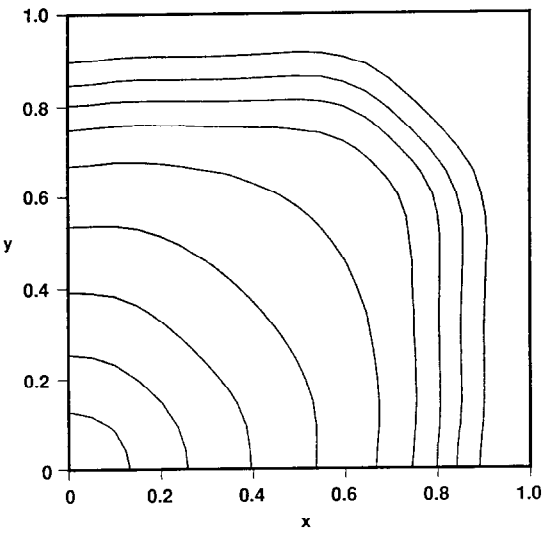

FIG. 18. Water saturation profiles from higher order solution of the Buckley–Leverett equation.

4. POSSIBLE EXTENSIONS

Other limiting procedures are quite feasible and should be tested. Our compressive limiter is not a direct analogue of superbee, since superbee (and many other limiters [19]) occasionally allows values other than zero or any of the slopes being compared to be the final choice of slope (or gradient in our two-dimensional case).

A more significant issue is the treatment of diffusive terms. In this case, the governing equation is of the form

$$u_t + \nabla \cdot \mathbf{F}(u) = \varepsilon(u_{xx} + u_{yy}), \qquad \varepsilon > 0. \tag{4.1}$$

The discrete analogue of (2.3) now involves the additional term,

$$\frac{\varepsilon}{|\Delta_{ABC}|}\left(\int_{l_{AB}} \frac{\partial u}{\partial n}\, dl + \int_{l_{AC}} \frac{\partial u}{\partial n}\, dl + \int_{l_{BC}} \frac{\partial u}{\partial n}\, dl\right), \tag{4.2}$$

on the right side of (2.3). Up to first-order accuracy, we compute each of the three terms in (4.2) as follows. The limiting procedure has already given us a gradient within the triangle ABC as well as for each of the three neighbors. Therefore, the integral along side AB in (4.2) can be computed approximately as

$$[(\nabla L_{ABC} + \nabla L_{ABF}) \cdot \mathbf{n}]\frac{l_{AB}}{2}. \tag{4.3}$$

The integrals along the other sides are approximated analogously. This is generally a first-order accurate method (second-order accuracy occurs in special cases, e.g., if all the triangles are equilateral). However, since ε is relatively small here (otherwise transport is diffusion dominated and the sophisticated treatment of convection is unnecessary), we believe this to be an adequate treatment of these terms.

Finally, we mention that work is underway to approximate (2.1) using a higher order accurate ENO triangle based method. See [20, 22] for successful Cartesian coordinate approaches.

ACKNOWLEDGMENT

We thank B. Cockburn for insightful comments on an earlier draft of this paper.

REFERENCES

1. A. Harten, *Math. Sci. Res. Inst. Publ., Vol. 7*, edited by A. Chorin and A. Majda (Springer-Verlag, New York/Berlin, 1987), p. 147.
2. S. Osher and P. K. Sweby, *IMA Conference Series, Vol. 9*, edited by A. Iserles and M. J. D. Powell (Clarendon, London/New York, 1987), p. 681.
3. J. P. Boris and D. L. Book, *J. Comput. Phys.* **11**, 38 (1973).
4. A. Harten, S. J. Osher, B. Engquist, and S. R. Chakravarthy, *J. Appl. Numer. Math.* **2**, 347 (1986).
5. A. Harten, B. Engquist, S. J. Osher, and S. R. Chakravarthy, *J. Comput. Phys.* **71**, 231 (1987).
6. R. Sanders, *Math. Comput.* **51**, 535 (1988).
7. S. Osher, *SIAM J. Numer. Anal.* **22**, 947 (1985).
8. B. Van Leer, *J. Comput. Phys.* **14**, 361 (1974).
9. A. Jameson, *Computational Mechanics—Advances and Trends, Vol. 75*, edited by A. K. Noor (Amer. Soc. Mech. Eng., New York, 1986), p. 329.
10. R. Löhner, K. Morgan, M. Vahdati, J. P. Boris, and D. L. Book, *Commun. Appl. Numer. Methods* **4**, 717 (1988).
11. R. R. Thareja, R. K. Prabhu, K. Morgan, J. Peraire, J. Peiro, and S. Soltani, AIAA Paper 90-0395, 1990 (unpublished).
12. P. Rostand and B. Stoufflet, *Notes on Numerical Fluid Mechanics Vol. 24*, edited by J. Ballmann and R. Jeltsch (Vieweg, Weisbaden, 1988), p. 510.
13. T. J. R. Hughes and T. Tezduyar, *Comput. Methods Appl. Mech. Engrg.* **45**, 217 (1984).
14. G. Chavent, G. Cohen, J. Jaffre, R. Eymard, D. R. Guerrillot, and L. Weill, *SPE Res. Eng.* 567 (Nov. 1990).
15. J. B. Goodman and R. J. LeVeque, *Math. Comput.* **45**, 15 (1985).
16. S. J. Osher, *SIAM J. Numer. Anal.* **21**, 217 (1984).
17. E. Tadmor, *Math. Comput.* **43**, 369 (1984).
18. S. Osher, *Analytical and Numerical Approaches to Asymptotic Problems in Analysis, Vol. 47*, edited by S. Axelsson, L. S. Frank, and A. van der Sluis (North Holland, Amsterdam, 1981), p. 179.
19. P. K. Sweby, *SIAM J. Numer. Anal.* **21**, 995 (1984).
20. C.-W. Shu and S. J. Osher, *J. Comput. Phys.* **77**, 439 (1988).
21. D. W. Peaceman, *Fundamentals of Numerical Reservoir Simulation* (Elsevier, Amsterdam, 1977).
22. C.-W. Shu and S. J. Osher, *J. Comput. Phys.* **83**, 32 (1989).